Strange Kinetics of the C_2H_6 + CN Reaction Explained†

Yuri Georgievskii*

Combustion Research Facility, Sandia National Laboratories, Livermore, California 94551-0969

Stephen J. Klippenstein‡

Chemistry Division, Argonne National Laboratory, Argonne, Illinois 60439

Received: December 7, 2006; In Final Form: February 1, 2007

In this paper, we employ state of the art quantum chemical and transition state theory methods in making a priori kinetic predictions for the abstraction reaction of CN with ethane. This reaction, which has been studied experimentally over an exceptionally broad range of temperature (25−1140 K), exhibits an unusually strong minimum in the rate constant near 200 K. The present theoretical predictions, which are based on a careful consideration of the two distinct transition state regimes, quantitatively reproduce the measured rate constant over the full range of temperature, with no adjustable parameters. At low temperatures, the rate-determining step for such radical−molecule reactions involves the formation of a weakly bound van der Waals complex. At higher temperatures, the passage over a subthreshold saddle point on the potential energy surface, related to the formation and dissolution of chemical bonds, becomes the rate-determining step. The calculations illustrate the changing importance of the two transition states with increasing temperature and also clearly demonstrate the need for including accurate treatments of both transition states. The present two transition state model is an extension of that employed in our previous work on the C_2H_4 + OH reaction [*J. Phys. Chem. A* **2005**, *109*, 6031]. It incorporates direct ab initio evaluations of the potential in classical phase space integral based calculations of the fully coupled anharmonic transition state partition functions for both transition states. Comparisons with more standard rigid-rotor harmonic oscillator representations for the "inner" transition state illustrate the importance of variational, anharmonic, and nonrigid effects. The effects of tunneling through the "inner" saddle point and of dynamical correlations between the two transition states are also discussed. A study of the kinetic isotope effect provides a further test for the present two transition state model.

I. Introduction

For many radical−molecule reactions,

$$R + M \rightarrow A \tag{1}$$

the high-pressure rate constant features a negative temperature dependence at low temperatures; i.e., the rate constant decreases with increasing temperature. In eq 1 R is the radical species, M is the molecule, and A denotes a chemical adduct that may be subject to further chemical transformations. Negative temperature dependences have been reported for reactions of olefins with Cl,[1−4] O(^{3}P),[5−9] OH,[10−14] CN,[15] and NH[16] radicals and many other reactions.

This unusual temperature dependence has often been explained in terms of a barrier separating the reactants from the adduct, with a barrier energy, $V^{\ddagger}$, that is less than that of the reactants.[17] A schematic diagram illustrating the expected potential energy surface is provided in Figure 1. Then, a simple Arrhenius-type formula,

$$k = Ae^{-V^{\ddagger}/k_BT} \tag{2}$$

provides the requisite temperature dependence. Equation 2, however, has a considerable drawback: it diverges exponentially as the temperature goes to zero.

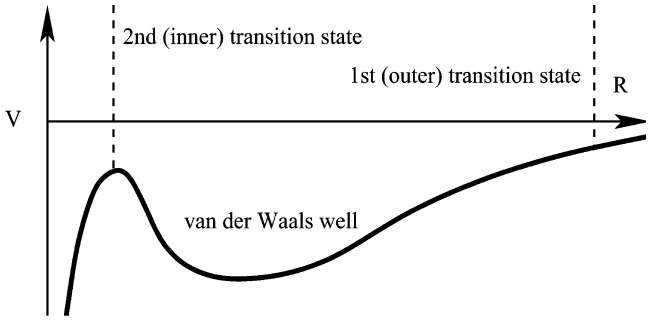

Figure 1. Schematic one-dimensional picture of the potential as a function of the reaction coordinate.

This unphysical behavior is related to the fact that, in deriving eq 2, one assumes that the transition state for reaction 1 lies in the vicinity of the barrier with negative energy $V^{\ddagger}$ for all temperatures. It is clear, however, that at low enough temperatures a variational treatment would favor the "outer" transition state that corresponds to a large interfragment distance and weak long-range interactions between the fragments. Even though this "outer" transition state is looser, with a larger prefactor A in eq 2, it has a smaller, by absolute value, activation energy, which is most important at low temperatures. Thus, at relatively high temperatures the "inner" transition state, which lies at the barrier, controls the reaction rate, and at extremely low temperatures

† Part of the special issue "James A. Miller Festschrift".

* Corresponding author. E-mail: ygeorgi@sandia.gov.
‡ E-mail: sjk@anl.gov.

10.1021/jp068430k CCC: $37.00
Published on Web 03/20/2007

the "outer" transition state provides the primary "bottleneck" for the reaction.[18,19]

To calculate the rate constant in the intermediate range of temperatures, one must consider the formation of a van der Waals complex C followed by its competing redissociation and/or transformation into a chemical adduct,[20−24]

$$R + M \rightleftharpoons C \rightarrow A \tag{3}$$

The calculation of the rate constant of reaction 3 is considerably simplified by the fact that the van der Waals complex C is weakly bound and therefore relatively short-lived. As a result, for all but extraordinarily high pressures the kinetics of this complex occurs in a collisionless regime with the total energy E and angular momentum J conserved. (Some interesting examples of deviations from this collisionless limit have been provided in the recent work of Luther and Troe and coworkers.[25−27])

A general expression for the rate constant can then be obtained by the following argument.[20] The inner and outer transition states act as a sequence of filters for reaction 3. The rate of forming complex C from the reactants with a given total energy E and angular momentum J is proportional to the number of states $N_1^{\ddagger}(E,J)$ of the corresponding transition state (cf. Figure 1). Complex C, once it has been formed, can either redissociate back to reactants or proceed on to the chemical adduct A. The branching ratio $\beta(E,J)$ for this process is given by

$$\beta(E,J) = \frac{N_2^{\ddagger}(E,J)}{N_1^{\ddagger}(E,J)} \tag{4}$$

where $N_2^{\ddagger}(E,J)$ is the number of states for the second transition state; cf. Figure 1. Then the rate for forming the chemical adduct A is proportional to $\beta(E,J)\, N_1^{\ddagger}(E,J)/(1 + \beta(E,J))$, which can be called an effective number of states $N_{\mathrm{eff}}^{\ddagger}(E,J)$ for the complex reaction 3,

$$N_{\mathrm{eff}}^{\ddagger}(E,J) = \frac{N_1^{\ddagger}(E,J)\, N_2^{\ddagger}(E,J)}{N_1^{\ddagger}(E,J) + N_2^{\ddagger}(E,J)} \tag{5}$$

The "high pressure" rate constant for reaction 3 is then obtained from the standard Boltzmann averaging of $N_{\mathrm{eff}}^{\ddagger}(E,J)$,

$$k^{\infty}(T) = \frac{1}{hQ_{\mathrm{reactants}}} \int N_{\mathrm{eff}}^{\ddagger}(E,J) \mathrm{e}^{-E/k_B T}\, \mathrm{d}E\, \mathrm{d}J \tag{6}$$

where we assume that the pressure is high enough to stabilize the chemical adduct before it redissociates, but not so high that the van der Waals complexes experience any collisions.

The implementation of eq 6 for a specific reaction requires prescriptions for evaluating both $N_1^{\ddagger}(E,J)$ and $N_2^{\ddagger}(E,J)$. Various procedures for doing so have been employed in past studies of radical molecule reactions.[20−22,24,28] These studies have generally employed fixed transition state rigid-rotor harmonic oscillator treatments of the inner transition state coupled with crude approximations for the outer transition state. At low temperatures the rigid-rotor harmonic-oscillator treatment should be a reasonable approximation for the inner transition state, which lies in the vicinity of the saddle point on the potential energy surface. However, at higher temperatures anharmonic and variational effects may become important for some of the low-frequency so-called transitional modes, which correlate with the free rotations and translations of the fragments. Quantitative treatments of the outer transition state are, of course, key to correctly predicting the low temperature behavior, as well as the transition from it to high temperature. A recent theoretical approach,[29] which has been termed modified transition state theory, takes a particularly simple view, by considering only the effect of the outer transition state on the threshold energies for the reaction. The latter approach should not be expected to yield accurate rate coefficients in the low and intermediate temperature regimes.

In our recent two transition state (2TS) study[23] of the OH + C_2H_4 reaction we have incorporated more accurate a priori models for both the inner and outer transition states. Two separate treatments of the inner transition state were considered. In particular, variational effects at the inner transition state were considered within the reaction path Hamiltonian approach.[30−33] The advantage of this approach is that computationally it is relatively inexpensive and it allows one to treat all nonreactive modes on the same footing. The drawback is that the ability to treat global anharmonic effects is quite limited. Hindered rotor models can be used to treat anharmonic effects for some, but not all, of the modes.[23] The alternative approach employed a direct ab initio evaluation of the potential in determining the contribution to the number of states from the transitional modes via Monte Carlo integration of the configurational integral representation for the partition function.[34−37] This approach builds on our related work for radical−radical reactions, where we have found that direct CASPT2 potential samplings yield transitional mode contributions that provide predictions for the capture rate that appear to be accurate to about 10−20%.[38,39]

The outer transition state lies beyond the van der Waals minimum, at large separations where only long-range interactions are important. Considerable effort has been devoted to the implementation of quantized versions of transition state theory for long-range potentials at low temperatures.[18,19] These methods are rather sophisticated, require major computational effort, and are restricted to specific forms for the potentials. As a practical alternative, we have recently developed a simplified version of classical variational transition state theory appropriate for large separations between the fragments.[40] This theory is applicable to any type of long-range potential and is still accurate for all practically important temperatures (e.g., $T \gtrsim 10$ K). Here, we will use this long-range transition state theory in calculating the number of states for the outer transition state.

In this paper we apply 2TS model calculations to the reaction of CN radical with ethane. This reaction provides an excellent test case for the 2TS model for a variety of reasons. First, because this reaction proceeds via a hydrogen abstraction mechanism,

$$C_2H_6 + CN \rightarrow C_2H_5 + HCN \tag{7}$$

there is no stabilization of chemical intermediates. Correspondingly, there is no ambiguity about whether or not the high-pressure limit for this reaction has been reached, which often hampers the comparison of theory with experiment. More importantly, the experimental data for this reaction are available for an unusually broad range of temperatures.[15,41−44] Using the CRESU technique pioneered in Rowe's laboratory,[45] Sims et al. measured the rate constant for the reaction of CN with C_2H_6 down to the ultralow temperature of 25 K.[15] Meanwhile, Balla et al.[43] have obtained experimental data for temperatures as high as 1140 K. Furthermore, a variety of studies have measured the rate coefficient near room temperature, with all of the studies being fairly consistent with each other. Overall, the various

experimental results provide a highly consistent description of the rate coefficient all the way from 25 to 1140 K.

The rate constant for reaction 7 has a very unusual temperature dependence: Starting from the high value of 10^{-10} cm^3 molecule^{-1} s^{-1} at 25 K, it decreases monotonically until it reaches its minimal value of 2×10^{-11} cm^3 molecule^{-1} s^{-1} at 200 K. With a further increase in temperature, the rate constant rises monotonically, reaching a value of 10^{-10} cm^3 molecule^{-1} s^{-1} at about 1000 K. The apparent explanation for this remarkable behavior lies in the fact that, due to the high electron affinity of the CN radical,[46] the potential barrier for the hydrogen abstraction is close to zero. Smith and co-workers have suggested that a transient van der Waals complex plays an important role in the mechanism.[15,47] However, to the best of our knowledge, no quantitative calculations have ever been performed to validate this perspective.

The CN + C_2H_6 reaction is also of interest for some purely theoretical reasons. In contrast with the reactions of OH, O(^{3}P), and Cl radicals, there are no low-energy excited spin−orbit states for CN. Thus, the reaction dynamics occurs on a single, doubly degenerate electronic surface and there is no uncertainty related to the possibility of nonadiabatic transitions between different electronic states. Furthermore, the relatively small size of the two reactants allows for the implementation of fairly sophisticated electronic structure methods in the analysis of the saddle point and reaction path properties. This small size also decreases the computational requirements for the direct sampling evaluations.

Due to all these factors reaction 7 is a perfect candidate for quantitative testing of the 2TS model. In section II we describe the details of the electronic structure calculations and transition state theory methods employed here. Separate descriptions are provided for the two different treatments of the inner transition state and in addition for the treatment of the outer transition state. The results and discussion are presented in section III. This discussion focuses on the effects of the two transition states and includes a detailed comparison with the experimental results, including those for the kinetic isotope effect. The importance of various factors such as the anharmonicities, tunneling, dynamical correlations, and variational effects are also discussed. In section IV some general conclusions are made.

II. Computational Methodology

The inner transition state lies in the vicinity of the saddle point on the potential energy surface. At low temperatures the rigid-rotor harmonic-oscillator (RRHO) treatment is a reasonable approximation for the inner number of states. At higher temperatures anharmonic and variational effects become important. Two different methods are used to treat these effects.

A. Inner Transition State: Reaction Path Hamiltonian Approach. In this approach the number of states is evaluated for a set of points along the minimum energy path by calculating the projected frequencies and then performing a direct sum over the rigid-rotor harmonic-oscillator energies. The so obtained number of states is then minimized with respect to the points on the minimum energy path for each value of the energy and total angular momentum.

The quantitative implementation of this approach requires accurate ab initio evaluations of the energies and vibrational frequencies in the vicinity of the saddle point along the minimum energy path. To begin, we have determined the geometry for the abstraction saddle point with both restricted open shell quadratic configuration interaction with the perturbative contributions of connected triple excitations[48,49] [RQCISD(T)] and with second-order multireference perturbation theory[50,51] (CASPT2). All of the quantum chemistry calculations described in this section were performed with the Molpro software package.[52] The recent implementation in Molpro of analytic gradients for the CASPT2 method[53] greatly facilitates these calculations.

These geometry optimizations, and subsequent single-point energy evaluations, employed Dunning correlation-consistent, polarized basis sets of different orders.[54] Because the saddle point geometry of reaction 7 is fairly loose, the use of diffuse basis functions is essential for geometry optimizations and the augmented double- ζ basis set (ADZ) was used for most of the calculations. A CASPT2 saddle point optimization with the augmented triple-ζ basis set (ATZ) yielded an essentially identical geometry to that obtained with the ADZ basis set.[55] Furthermore, energy profiles calculated along the minimum energy path, which itself was obtained with the CASPT2/ADZ method, are fairly similar for different basis sets. Thus, the ADZ basis set was deemed sufficient for the saddle point optimization, force constant, and energy profile calculations along the minimum energy path.

For the QCISD(T) calculations, a fairly large Q1 diagnostic[56] of 0.033 is calculated for the saddle point. This moderately large value is, apparently, related to the significant multireference character of the wave function for the CN radical, whose Q1 diagnostic of 0.068 is even larger.

The CASPT2 approach provides a means for examining the possible effect of these multireference characters. The focus of these CASPT2 calculations was on obtaining an accurate treatment of the CN radical. The geometries of the fragments do not change considerably from the reactants to the transition state. Thus, it is reasonable to use as a complete active space (CAS) for the preceding CASSCF calculation[57,58] only the orbitals that correlate with those of the CN radical. We have explored a variety of different active spaces. Including just the π and π^* orbitals of CN along with the radical orbital in a five-electron, five-orbital (5e,5o) CAS does not provide a sufficiently accurate description of either the geometry or the energy at the inner potential barrier. The inclusion of both the σ and σ^* orbitals of CN, to yield a (7e,7o) active space, gives a saddle point geometry that is in reasonably satisfactory agreement with that from the RQCISD(T)/ADZ calculation. Interestingly, simply adding a single doubly occupied A′ orbital to the (5e,5o) space yielded a geometry that is essentially identical to that from the RQCISD(T)/ADZ calculation. The extra orbital in this (7e,6o) case is a hybrid of the σ CN bond and a nitrogen lone pair. A possible explanation for this improved agreement may be related to the importance of including the nitrogen lone pair orbital in the active space, which is partially done with the (7e,6o) scheme, but not with the (7e,7o) scheme. Some attempt was also made to add the N lone pair orbitals to the (7e,7o) active space, but it was found that some of the CH σ and σ^* orbitals then began to mix in.

The C_s saddle point geometry obtained with the CASPT2-(7e,6o)/ADZ approach is illustrated in Figure 2. The saddle point is seen to be very early, with almost no deviation from the CN, CH, or CC bond lengths in the free fragments. The saddle point energies calculated with the CASPT2(7e,6o), RQCISD(T), and the open shell coupled-cluster method with perturbative triples contribution, RCCSD(T),[59] at these CASPT2(7e,6o)/ADZ geometries are compared in Table 1. The three methods are seen to be remarkably consistent, differing by less than 0.12 kcal/mol for the ADZ basis set. This good agreement lends

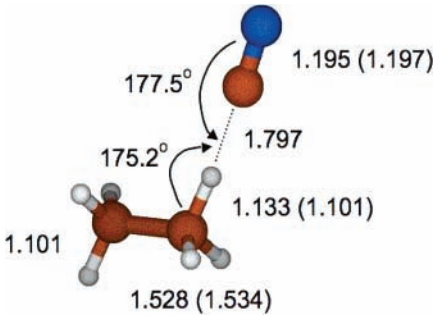

Figure 2. Saddle point geometry for the $C_2H_6\cdots$CN abstraction transition state optimized with the CASPT2(7e,6o)/ADZ method. Bond lengths are in angstroms, and bond angles, in degrees. The numbers in parentheses denote the corresponding bond lengths for free CN and C_2H_6.

TABLE 1: Saddle Point Energy

basis	CASPT2(7e,6o)[a]	RQCISD(T)[a]	RCCSD(T)[a]
ADZ	−0.096	−0.208	−0.135
ATZ	0.170	0.105	0.057
AQZ	0.378	0.345	0.264
∞	0.522	0.512	0.408
DZ	1.304	1.373	1.440
TZ	0.740	0.738	0.695
QZ	0.602	0.580	0.500
5Z	0.570	0.528	0.435
∞	0.54	0.480	0.374

[a] All energies are in kcal/mol relative to reactants, are for the optimized geometries obtained with the CASPT2(7e,6o)/ADZ method, and do not include any zero-point corrections.

confidence in the correctness of the energy estimates for each of these methods.

The basis set dependence of the saddle point energies from these three methods is also reported in Table 1. Two series of energies, one corresponding to the regular double-, triple-, quadruple-, and pentuple-ζ basis sets and the other to the augmented double-, triple-, and quadruple-ζ series are considered. The results for these specific basis sets are also extrapolated to the infinite basis set limit according to the expression[60,61]

$$E_l = E_\infty + B/(l+1)^4 \quad (8)$$

using the last two energies in each series, where l denotes the maximum angular momentum quantum number in the basis set and B is a fitting parameter. For (A)TZ, (A)QZ, and 5Z, l is equal to 3, 4, and 5, correspondingly. Remarkably, each of these methods seem to converge to the same infinite basis set limit. In the following rate calculations, we take the RRCSD(T) limit of $E_{HL} = 0.41$ kcal/mol. The remaining calculations are within 0.13 kcal/mol of this value, although in reality the uncertainty in this value is likely much greater, perhaps on the order of ±0.5 kcal/mol.

The relative computational efficiency of the CASPT2(7e,6o) approach, coupled with its good agreement with the RQCISD(T) geometries and energies led us to employ this method in the remainder of the reaction path geometry and frequency evaluations. The CASPT2(7e,6o)/ADZ calculated vibrational frequencies for the reactants, the saddle point, and van der Waals complex are reported in Table 2. The minimum energy path has been obtained using the quadratic steepest descent reaction path following method.[62,63] The vibrational frequencies for the nonreactive modes, which are orthogonal to the reaction path, are obtained from a reoriented optimized dividing surface (RODS) calculation[64] implemented in the POLYRATE program.[65] The force constants along the minimum energy path are calculated with the CASPT2(7e,6o)/ADZ method. A one-dimensional Eckart model is used to estimate the quantum effects related to the tunneling through the barrier along the unstable reactive mode.

B. Inner Transition State: VRC−TST Approach. At higher temperatures anharmonic effects are likely to become important for some of the so-called transitional modes, which have low frequencies and correlate with the rotations and relative translations of the free fragments. Simple hindered rotor models can sometimes be used to account for these anharmonic effects.[23,32] For reaction 7, however, it is not clear how to correlate the low-frequency transitional modes with any specific internal rotation. An alternative approach involves the direct numerical integration of the classical phase space expression for the transitional mode number of states, as in the VRC-TST method developed for studying the kinetics of radical−radical reactions.[34−37]

Application of this VRC-TST approach to radical−molecule reactions such as reaction 7 presents certain difficulties related to the fact that the inner transition state is now at significantly shorter separations. As a result, the presumed separation between the conserved vibrational modes of the fragments[66] and the transitional modes is not as appropriate. Thus, it now becomes important to consider, at least to first order, the effect of the couplings between conserved and transitional modes. For the present reaction, this primarily involves the relaxation of the conserved mode coordinates for each of the geometries sampled during the numerical integration over the transitional modes.[23]

The direct sampling method is fairly computationally intensive, particularly for reactions such as the present one, where the transition state lies at fairly short separations with a correspondingly small flux. Thus, thousands of samplings are required for each dividing surface that is considered. Furthermore, the conserved mode geometries must be internally relaxed for each of these thousands of configurations. As a result, only relatively inexpensive quantum chemistry methods can be used for the direct sampling part of the calculation. Here, unrestricted second-order Møller−Plesset perturbation theory (UMP2) with a 6-31G* basis set is used for this direct sampling. The

TABLE 2: Vibrational Frequencies and Energies for the Stationary Points

species	vibrational frequencies[a]	ΔE_0[b]	E[c]
saddle point	212i, 39, 54, 97, 136, 348, 806, 813, 1033, 1174, 1205, 1339, 1394, 1396, 1459, 1485, 1490, 2020, 2380, 3067, 3101, 3154, 3159, 3180	−0.89	0.41
van der Waals minimum	17, 25, 64, 65, 77, 325, 812, 815, 1028, 1210, 1212, 1384, 1411, 1490, 1493, 1494, 1497, 2002, 3060, 3065, 3138, 3140, 3160, 3164	0.28	−0.91[d]
C_2H_6	321, 816, 816, 1030, 1213, 1213, 1384, 1413, 1495, 1495, 1495, 1495, 3068, 3070, 3146, 3146, 3167, 3167		
CN	2004		

[a] Frequencies (in cm^{-1}) were calculated with the CASPT2(7e,6o)/ADZ method. [b] Change in the zero-point energy from reactants in kcal/mol [c] Electronic energy relative to reactants [d] Calculated with CASPT2(7e,6o) extrapolated to the complete basis set limit and evaluated at the ADZ geometry.

GAUSSIAN98 program is used in these UMP2/6-31G* evaluations.[67] Of course, the UMP2/6-31G* method does not provide particularly accurate saddle point or reaction path energies. This inadequacy is corrected for via the incorporation of one-dimensional corrections based on the CASPT2/ADZ minimum energy path energies and the estimated saddle point energy of 0.41 kcal/mol.

It is also important to consider the variations in the conserved mode vibrational frequencies, which depend on the mutual orientation and the distance between the reactants. For reaction 7 most of the conserved modes frequencies for the reactive complex are too high to be excited in the considered range of temperatures. As a result, the main effect of the conserved modes on the inner number of states is related to the change in the zero-point energy at the transition state relative to the reactants at infinite separation. As we will see, the zero-point energy of the conserved modes for reaction 7 strongly depends on the distance between the reactants.

This conserved mode zero-point energy was calculated with the CASPT2(7e,6o)/ADZ method along the minimum energy path and then used together with the one-dimensional electronic energy correction to modify the effective potential energy for the transitional modes. The frequencies of the normal modes are obtained from the second derivatives of the potential which are numerically calculated for a set of points along the MEP. The lowest 11 modes corresponding to the reactive mode, 6 translational and rotational modes, and 4 transitional modes are excluded, and the rest are designated as conserved ones. The zero-point energy is obtained as a half-sum of the conserved modes frequencies. This zero-point energy correction will be seen to have an important role in the analysis of the kinetic isotope effect.

Reaction 7 can proceed through six equivalent channels. Thus, a multifaceted dividing surface with six pivot points corresponding to these channels is used to optimize the inner number of states for this reaction.[36] We have studied the effect of the pivot point position on the inner number of states. To this end, we put six equivalent pivot points along the C−H bonds of the C_2H_6 molecule, with a variable distance d between the pivot points and the nearest carbon atom of the C_2H_6 molecule. For each face of the multifaceted surface associated with a given d, we have also fixed the distance r between the pivot point and the carbon atom of the CN radical so that the maximum C−C distance R_{CC} between the C atom of the CN radical and the corresponding C atom of the C_2H_6 molecule is 5.68 bohr. This R_{CC} value corresponds approximately to the saddle point configuration after the zero-point correction.

In Figure 3 the inner transition state rate constants calculated for d values ranging from 1.5 to 2.25 bohr are illustrated for temperatures ranging from 100 to 1000 K. The predicted rate constants are seen to decrease somewhat with increasing d values, but the extent of the dependence on d becomes quite small for d beyond 2.0 bohr. For d values beyond 2.5 bohr, the calculations become unstable, as the conserved mode optimizations begin to yield configurations in which the H atom has already transferred to the CN radical. Such configurations essentially correspond to configurations with greatly increased fluxes and so are not important variationally. The plots in Figure 3 suggest that the largest d values for which the calculations are stable should yield the variationally best rate. Overall, we have found that $d = 2$ bohr provides an optimal compromise between variational minimization and stability as we consider

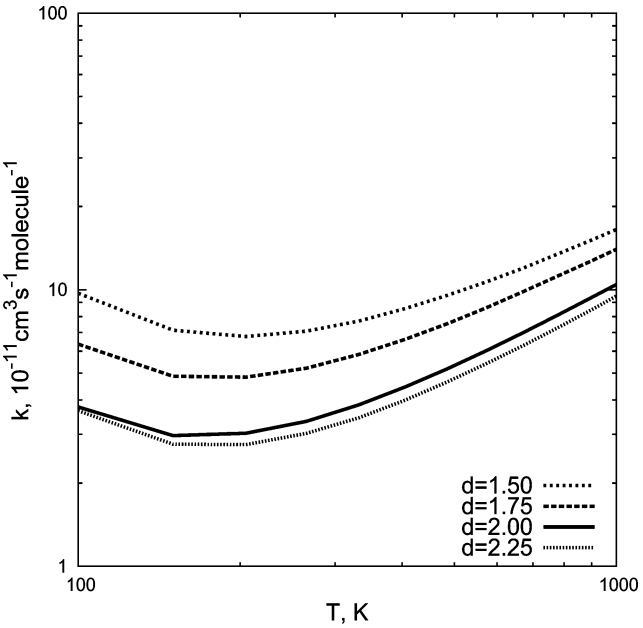

Figure 3. Reactive flux through the dividing surfaces corresponding to different pivot point positions.

other R_{CC} separations in the full calculation. This pivot point location is used in the final VRC-TST calculations presented below.

The VRC-TST approach is generally of limited applicability to abstraction reactions because the interfragment distance is not a good reaction coordinate. For reaction 7, however, which is characterized by a high exothermicity and low potential barrier, the transition state configuration corresponds to a relatively large separation between the reactants (cf. Figure 2). As a result, the transitional-conserved mode separation, which is a central assumption of the VRC-TST approach, provides a reasonable starting point. However, the applicability of the VRC-TST approach is still restricted to not very high temperatures. At too high temperature the character of the reaction coordinate changes from interfragment separation to the hydrogen transfer coordinate. As a result, the conserved mode describing the hydrogen abstraction becomes unstable and at sufficiently close CN−C_2H_6 separation the hydrogen "jumps" from C_2H_6 to CN. The critical C−C distance is about 5.1 bohr, which corresponds to the location of the canonical transition state for a temperature of about 3000−4000 K.

C. Outer Transition State. To calculate the outer transition state number of states, we use our recently derived long-range transition state theory,[40] which is a simplified version of variational transition state theory applicable at large fragment separations. This approach employs the distance between the centers of mass of the two fragments as a reaction coordinate. The sample applications of this approach[40] indicated that it is usually important to include several long-range asymptotic terms in the potential, such as multipole and dispersion interactions, to correcty reproduce the outer rate constant at temperatures higher than 20 K. Therefore, in this paper, instead of calculating different long-range potential energy terms separately, we simply estimate the outer rate by direct sampling of the transitional mode configurational space, again using the VRC-TST approach. For this calculation, however, the effect of the conserved modes is negligibly small and can be disregarded. Also, because chemical bonding effects at long-range are irrelevant, calculations employing restricted open-shell second-order Møller−Plesset perturbation theory[68] (RMP2)[69] with the ADZ basis set should be accurate enough.

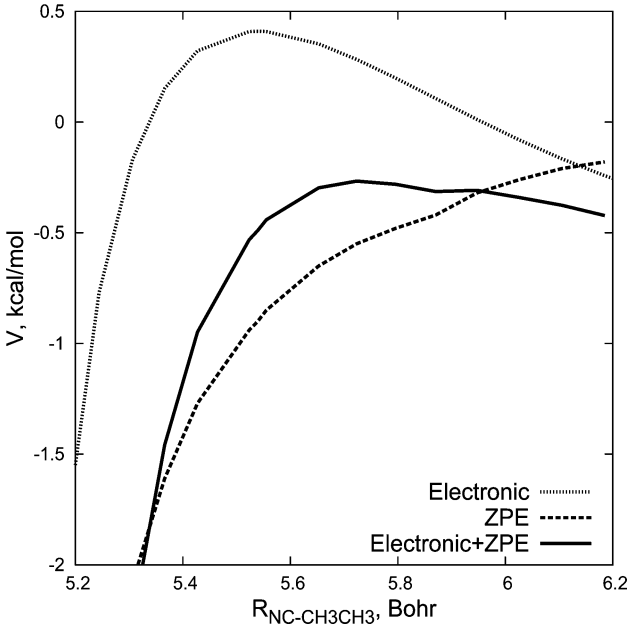

Figure 4. Electronic and zero-point energies along the minimum energy path shown as functions of the $NC-CH_3$ CH_3 distance in the vicinity of the saddle point. The dotted line corresponds to the electronic energy, the dashed line to the zero-point energy of nonreactive modes, and the solid line to the effective energy, which is the sum of the two.

We have found that within the framework of the two transition state approach the rate constant is usually not sensitive to the shape of the long-range potential as long as it correctly reproduces the outer rate constant in the important range of temperatures. Therefore, for simple bookkeeping reasons, the final two TS calculations replace the explicit long-range calculations with related calculations for an "equivalent" model long-range potential,

$$V(R) = -\frac{V_0}{R^6} \tag{9}$$

The advantage of this approach is that the analytical expression for $N(E,J)$ for the potential given by eq 9 is available.[40] With $V_0 = 359.1$ au, this expression provides a satisfactory reproduction of the RMP2/AVDZ based VRC-TST outer rate constant calculation for temperatures ranging from 20 to 200 K.

III. Results and Discussion

The electronic energy and the zero-point energy profiles for reaction 7 are shown in Figure 4. The electronic energy at the saddle point, 0.41 kcal/mol, lies slightly above the reactants level. However, the frequency of the breaking C−H bond at the saddle point is considerably lower than at infinite separation of the reactants, 2380 cm^{-1} versus 3068 cm^{-1}. The large negative zero-point energy correction to the electronic energy at the saddle point, −0.89 kcal/mol, yields a zero-point corrected saddle point energy of −0.48 kcal/mol. This negative energy implies that this reaction does indeed involve a prototypical two transition state mechanism. At higher temperatures the tighter inner transition state provides the dominant "bottleneck" for reaction 7, and at very low temperatures the looser outer transition state, which has, however, a less negative minimal energy, controls the rate constant; cf. Figure 5.

The results of our 2TS reaction path calculations for reaction 7 (cf. Figure 5) once again confirm an important general conclusion made before:[23] Taking account of the conservation

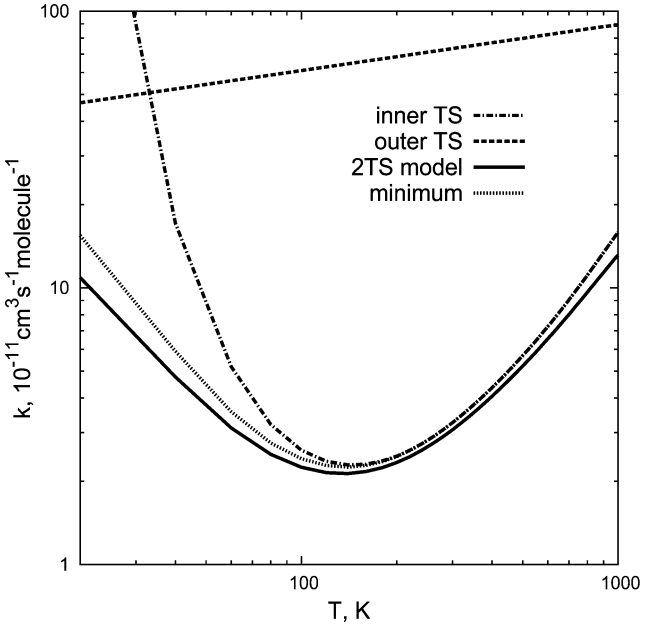

Figure 5. Inner, outer, 2TS model (eq 5), and minimum model (eq 11) rate constants as functions of temperature.

of total energy and total angular momentum for a reactive complex in the process of passing through its van der Waals well is crucial for quantitively estimating the rate constant of reaction 3. For example, in the temperature region between 20 and 40 K, where the inner and outer rate constants, k_1 and k_2, are of comparable magnitude, the E,J-resolved 2TS model rate constant is 4−5 times lower than a canonical approximation,[70,71]

$$k = \frac{k_1 k_2}{k_1 + k_2} \tag{10}$$

In deriving eq 5 one assumes that the van der Waals complex C has enough time to equilibrate and to "forget" from which state it came. Thus, the sequential crossings by the reactive complex of the transition states are considered to be uncorrelated events. This "ergodic assumption" may not always be completely correct, with its validity depending on factors such as the depth of the van der Waals well, and the configurations of the inner and outer transition states. It is difficult, however, to estimate this dynamical correlation effect quantitatively without detailed dynamical calculations. Nevertheless, one can estimate how large this effect might be by considering an opposite extreme. In particular, in the spirit of the adiabatic channel model of Troe,[72] one might presume that the reaction proceeds adiabatically along the reaction coordinate between the two transition states. In that case, the effective number of states is simply a minimum of the two for the inner and outer transition states,

$$N^{\ddagger}_{\min}(E,J) = \min(N^{\ddagger}_1(E,J), N^{\ddagger}_2(E,J)) \tag{11}$$

The rate constant estimates using both eq 5 and eq 11 are shown in Figure 5. One can see that even if the transition state crossings are completely correlated, which is highly improbable, the change of the rate constant is relatively small. Thus, one can reasonably assume that the dynamical correlation effect is not important for the calculation of rate constants for reaction 3.

The inner transition state variational and quantum tunneling effects for reaction 6 are illustrated in Figure 6. The comparison of the 2TS calculations with and without (fixed TS) the

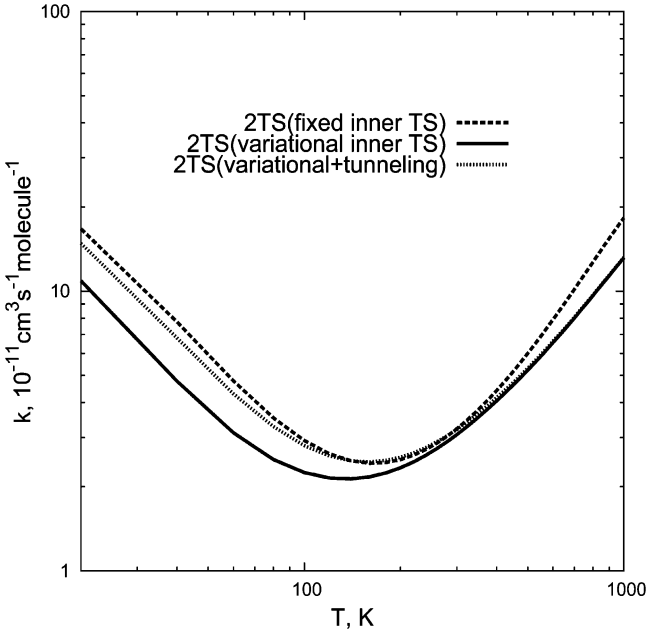

Figure 6. 2TS model rate constant of reaction 7 as a function of temperature. The inner number of states was calculated with the rigid-rotor harmonic-oscillator model at the saddle point (dashed line) and the reaction path Hamiltonian variation approach with (dotted line) and without (solid line) tunneling.

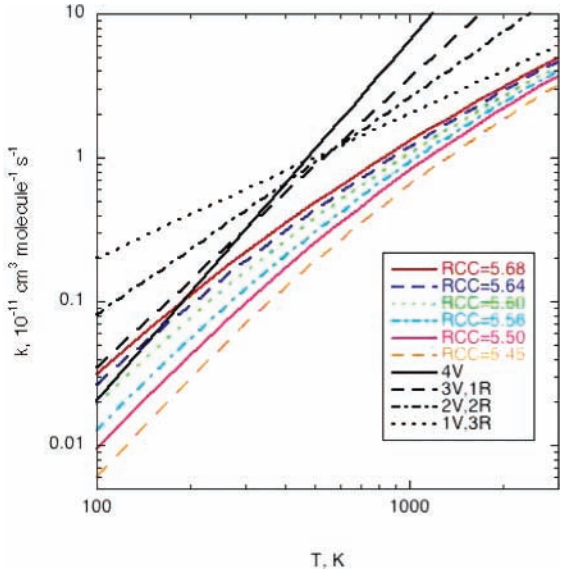

Figure 7. Effects of potential anharmonicity and nonrigidity on the reactive flux. The reference energy for each curve is the minimum energy on the corresponding divdiding surface. The four-vibrations, three-vibrations and one-rotation, two-vibrations and two-rotations, and one-vibrations and three-rotations models (arbitrary scaling) are also shown.

variational reaction path treatment for the inner transition state shows the effect of variational optimization within the reaction path Hamiltonian approach. The zero-point energy of reaction 7 strongly depends on the reaction coordinate, as can be seen from Figure 4. As a result, the maximum of the total energy is shifted relative to the saddle point and the RRHO analysis at the potential energy saddle point is not appropriate even at low energies or temperatures. Quantum tunneling effects, which correspond to the difference between the 2TS model calculations with and without tunneling, are relatively small for two reasons. First, because the effective potential barrier is negative, the main contribution to the reactive flux comes from the classically accessible region of energies. Second, the tunneling frequency at the saddle point is relatively low, 212 cm^{-1}, because the reactive mode corresponds mainly to carbon−carbon motion, and the related effective mass is relatively high. Nevertheless, the tunneling effect does still increase the overall rate by as much as 30% for temperatures near 40 K. Curiously enough, the variational effects, which decrease the rate constant, and the quantum tunneling effects, which increase it, almost cancel each other and the classical RRHO model for the inner transition state provides a reasonable estimate for the rate constant at $T \lesssim 300$ K.

At higher temperatures, $T \gtrsim 300$ K, a single inner transition state description can be used for the rate constant estimates. The frequencies of the transitional modes at the saddle point, 39, 54, 97, and 135 cm^{-1}, are rather low. With these low frequencies the parabolic approximation for the corresponding vibrational potentials, which is implicit in the rigid-rotor harmonic oscillator approximation for the energies, becomes inaccurate for this temperature region. In contrast, for C_2H_4 + OH these frequencies are 76, 231, 410, and 749 cm^{-1} and the parabolic approximation appeared to be adequate.[23]

To account for the anharmonic effects, we performed VRC-TST calculations as described in the previous section. In Figure 7 the reactive fluxes through a set of dividing surfaces in the vicinity of the saddle point are shown as a function of temperature. The central purpose of these plots is to illustrate how the temperature dependence varies from the behavior expected for four harmonic vibrations at low temperature to that expected for one vibration and three rotations at higher temperatures. To do so, the minimum energy on each dividing surface is used as a reference energy for the corresponding reactive flux calculation. With this choice for reference energy, the Boltzmann factors are removed, and the slope of each curve characterizes the effective shape of the potential. For comparison, lines (with arbitrary normalization) corresponding to the slopes expected for four vibrations, for three vibrations and one rotation, for two vibrations and two rotatations, and for one vibration and three rotations are also shown. As expected, at low temperatures the slopes of the curves appoach the slope corresponding to four vibrations, especially for more contracted (smaller R_{CC}) surfaces that have higher transitional mode frequencies. At higher temperatures, however, the slopes of the curves deviate from the four vibrations model, ultimately approaching the three-rotations one-vibration model at the highest temperature plotted. This transition clearly illustrates the necessity of an appropriate anharmonic treatment for this reaction at the higher temperatures.

The variational effects for the VRC-TST calculations are illustrated in Figure 8. For temperatures below about 350 K, the optimal canonical dividing surface passes through the zero-point corrected saddle point, which is at an R_{CC} of 5.7 bohr. Then at higher temperatures, the optimal R_{CC} value gradually decreases, reaching 5.3 bohr at a temperature of about 2000 K. At the latter temperature, the canonical VRC-TST rate coefficient for $R_{CC} = 5.3$ bohr is about 50% below that for $R_{CC} = 5.7$ bohr. From 100 to 2000 K, the E/J resolved VRC-TST rate coefficient and the 2 TS-model rate coefficients are consistently about 10 and 20% lower than the canonical ones, respectively, which is fairly typical.

In Figure 9 the calculated rate constant is compared with the available experimental data.[15,41−44] The dashed line corresponds to the 2TS model where the inner number of states is calculated with the reaction path Hamiltonian approach and includes a quantum tunneling correction. It reproduces the experimental data remarkably well for all $T \lesssim 200$ K. At higher temperatures

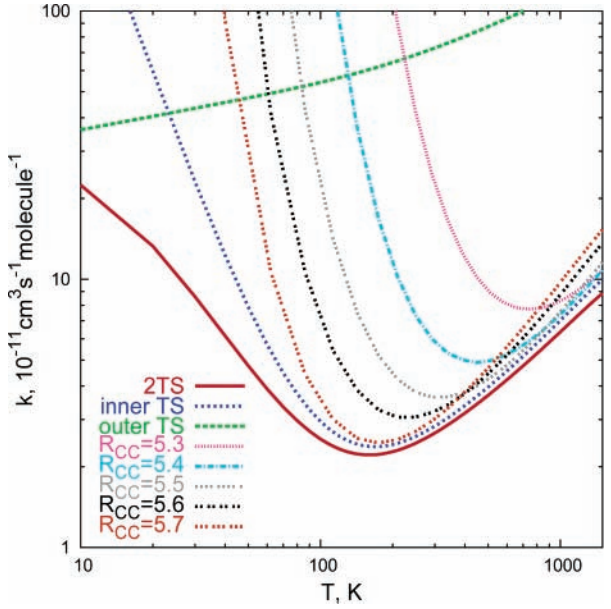

Figure 8. Plot of the variational effects for the VRC-TST calculations of the rate constant.

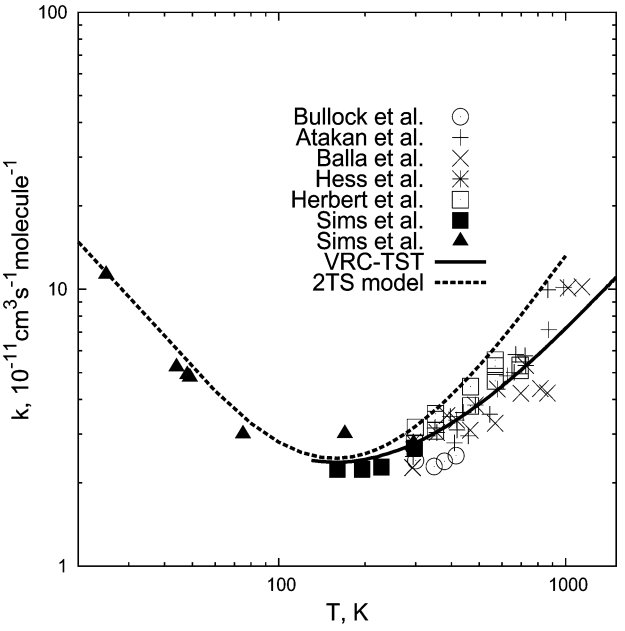

Figure 9. Rate constant of reaction 7 as a function of temperature. The dashed line corresponds to the 2TS model in which the reaction path Hamiltonian variational approach with tunneling correction is used for the inner transition state. The solid line corresponds to the VRC-TST treatment with one-dimensional zero-point and reaction path energy corrections.

anharmonic effects in the potential become important, and this model begins to overestimate the rate constant. In this region a single inner transition state model can be used; cf. Figure 6. To calculate the rate constant at $T \gtrsim 200$ K, we performed VRC-TST calculations with one-dimensional high-level electronic energy and zero-point energy corrections. The results of these VRC-TST calculations are represented by the solid line in Figure 9, which provides a satisfactory reproduction of the somewhat more disperse experimental data for this temperature range. Together, the 2TS model (with reaction path Hamiltonian treatment for the inner transition state) for low T and the VRC-TST inner transition state model for high T reproduce the rate constant of reaction 7 for the whole range of temperatures from 25 to 1140 K.

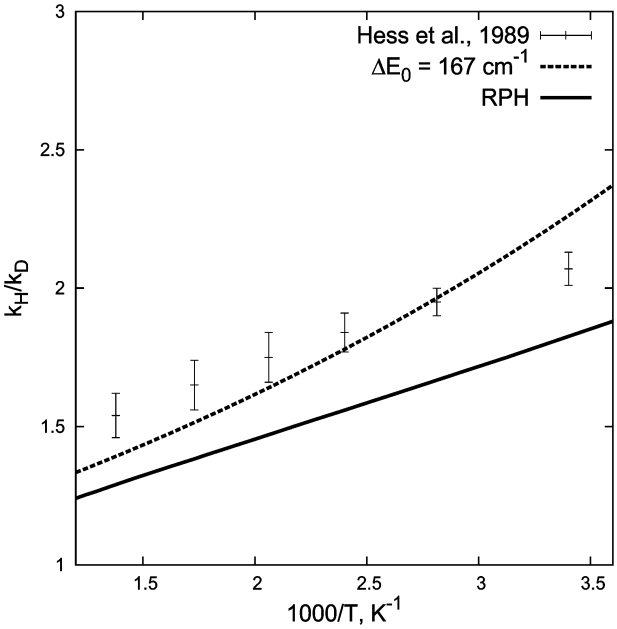

Figure 10. Ratio k_H/k_D of the rate constants for the reactions of CN with C_2H_6 and C_2D_6 as a function of temperature. The dashed line corresponds to eq 12, and the solid line is obtained with the reaction path Hamiltonian approach.

In the experiment of Sims et al.[15] the rate constant related to a loss of CN radical was observed at ultralow temperatures up to 25 K. At such low temperatures there is a possibility that in addition to formation of the products according to reaction 7 the reactive complex can be stabilized in the van der Waals well, thus effectively increasing the observed rate of the CN loss. To estimate this effect, we have performed a master equation calculation for reaction 3 with the van der Waals well parameters shown in Table 2. We found that the equilibrium constant of formation of the van der Waals complex from the reactants at the lowest experimental temperature of 25 K is about 0.7×10^{-17} cm^3. Thus, for the experimentally studied C_2H_6 concentration of 10^{14} cm^{-3}, the van der Waals well is too shallow to provide a measurable change in the CN concentration. Moreover, at the experimental pressure, which was about 0.1−0.2 Torr, and temperature of 25 K we found that the branching ratio between the formation of the van der Waals complex and the final products is negligibly small (less than 10^{-7}). Thus, our calculations strongly support the conclusion that in the experiment of Sims et al.[15] the overwhelming part of the CN loss is related to formation of HCN and C_2H_5 in reaction 7, even at the lowest temperature considered.

Hess et al.[41] have measured the rate constant for the reaction of CN with ethane and with its deuterated isotopes for temperatures ranging from 294 to 736 K. In Figure 10 we compare their results with two theoretical calculations. The observed kinetic isotope effect primarily arises from the difference in zero-point energies of the high-frequency modes for the deuterated and normal species. In the rigid-rotor harmonic oscillator approximation the ratio k_H/k_D of the rate constants for C_2H_6 and C_2D_6 molecules is approximately given by

$$k_H/k_D \simeq e^{-\Delta E_0/k_B T} \qquad (12)$$

where $\Delta E_0 = E_0^{\ddagger,H} - E_0^{\infty,H} - E_0^{\ddagger,D} + E_0^{\infty,D}$ is the difference in conserved mode zero-point energies change from the reactants to the transition state for C_2H_6 and C_2D_6 molecules. The dashed line in Figure 10 corresponds to eq 12 with $\Delta E_0 = 167$ cm^{-1}

calculated with the CASPT2(7e,6o)/ADZ method at the saddle point. A more accurate treatment, shown as a solid line, implements the full reaction path Hamiltonian approach. The latter treatment shows an improved temperature dependence but is about 20% too low. This modest discrepancy with the experimental results may simply be related to minor inaccuracies in the calculated zero-point energies and/or the saddle point energies.

IV. Concluding Remarks

The present theoretical calculations provide a convincing explanation for the sharp minimum in the rate coefficient for the CN + C_2H_6 reaction. As speculated by Sims and Smith,[15,47] the reaction proceeds through a van der Waals complex. The saddle point for abstraction lies below the energy of the reactants. Thus, at low temperatures the rate is determined by the rate for forming the van der Waals complex, which takes the large collision limit value of a few times 10^{-10} cm^3 $molecule^{-1}$ s^{-1}. With increasing temperature the inner transition state, corresponding to the abstraction saddle point, plays an increasingly important role, due to its much lower entropy. This increasing role of the inner transition state initially yields a reduction in the rate coefficient. Ultimately, however, at higher temperatures the small negative activation energy for the inner transition state becomes negligible. The temperature dependence is then determined by that of the partition function for the transitional modes.

The various comparisons presented here demonstrate that the quantitative description of this temperature dependence requires accurate descriptions of both the inner and outer transition states, including treatments of variational, anharmonic, and nonrigid effects for both TS's. As in our previous studies,[23] it was found that taking into account the energy and angular momentum conservation leads to an essential reduction of the rate constant in the transition region in comparison with both the inner and outer rates and is crucial for the quantitative prediction of the rate constant of reaction 7 at low temperatures.

The calculations presented in this paper reproduce experimental data remarkably well. They are, however, quite sensitive to the height of the potential barrier for the inner transition state $V^{\ddagger}$, and in general, it is difficult to reliably predict such barrier heights with an accuracy of better than 0.5−1 kcal/mol. However, if the rate constant is known at some temperature, one can use $V^{\ddagger}$ as the sole adjustable parameter in the prediction of the rate constant over a broad range of temperatures.

The present combination of VRC-TST and long-range transition state theory calculations of the rate coefficient can be expressed as the sum of modified Arrhenius forms, $7.30 \times 10^{-9}T^{-1.3} \exp(-3.116/T) + 4.25 \times 10^{-14}T^{1.068} \exp(61.51/T)$ cm^3 $molecule^{-1}$ s^{-1}, where the temperature T is in K. These results provide a remarkable reproduction of the experimental data over its full temperature range of 25−1140 K.

Acknowledgment. We acknowledge Larry Harding for helpful discussions. This work was supported by the U.S. Department of Energy, Office of Basic Energy Sciences, Division of Chemical Sciences, Geosciences, and Biosciences. Sandia is a multiprogram laboratory operated by Sandia Corp., a Lockheed Martin Company, for the United States Department of Energy under contract DE-AC04-94-AL85000. The work at Argonne was supported under DOE Contract Number DE-AC02-06CH11357.

References and Notes

(1) Bedjanian, Y.; Laverdet, G.; Bras, G. L. *J. Phys. Chem. A* **1998**, *102*, 953.
(2) Farrell, J. T.; Taatjes, C. A. *J. Phys. Chem. A* **1998**, *102*, 4846.
(3) Knyazev, V. D.; Kalinovski, I. J.; Slagle, I. R. *J. Phys. Chem. A* **1999**, *103*, 3216.
(4) Timerghazin, Q. K.; Ariya, P. A. *Phys. Chem. Chem. Phys.* **2001**, *3*, 3981.
(5) Singleton, D. L.; Furuyama, S.; Cvetanovic, R. J.; Irwin, R. S. *J. Chem. Phys.* **1975**, *63*, 1003.
(6) Davis, D. D.; Huie, R. E.; Herron, J. T. *J. Chem. Phys.* **1973**, *59*, 628.
(7) Gaffney, J. S.; Atkinson, R.; Pitts, J. N. *J. Am. Chem. Soc.* **1975**, *97*, 6481.
(8) Biehl, H.; Bittner, J.; Bohn, B.; Geers-Muller, R.; Stuhl, F. *Int. J. Chem. Kinet.* **1995**, *27*, 277.
(9) Weber, M.; Hake, A.; Stuhl, F. *Int. J. Chem. Kinet.* **1997**, *29*, 149.
(10) Atkinson, R. *Chem. Rev.* **1985**, *85*, 69.
(11) Sims, I. R.; Smith, I. W. M.; Bocherel, P.; Defrance, A.; Travers, D.; Rowe, B. R. *J. Chem. Soc., Faraday Trans.* **1994**, *90*, 1473.
(12) Vakhtin, A. B.; Lee, S.; Heard, D. E.; Smith, I. W. M.; Leone, S. R. *J. Phys. Chem. A* **2001**, *105*, 7889.
(13) Vakhtin, A. B.; Murphy, J. E.; Leone, S. R. *J. Phys. Chem. A* **2003**, *107*, 10055.
(14) Spangenberg, T.; Köhler, S.; Hansmann, B.; Wachsmuth, U.; Abel, B.; Smith, M. A. *J. Phys. Chem. A* **2004**, *108*, 7527.
(15) Sims, I. R.; Queffelec, J.-L.; Travers, D.; Rowe, B. R.; Herbert, L. B.; Karthauser, J.; Smith, I. W. M. *Chem. Phys. Lett.* **1993**, *211*, 461.
(16) Mullen, C.; Smith, M. A. *J. Phys. Chem. A* **2005**, *109*, 1391.
(17) Villa, J.; Gonzalez-Lafont, A.; Lluch, J. M.; Corchado, J. C.; Espinosa-Garcia, J. *J. Chem. Phys.* **1997**, *107*, 7266.
(18) Clary, D. C. *Ann. Rev. Phys. Chem.* **1990**, *41*, 61.
(19) Troe, J. *Adv. Chem. Phys.* **1997**, *101*, 819.
(20) Mozurkewich, M.; Benson, S. W. *J. Phys. Chem.* **1984**, *88*, 6429.
(21) Chen, Y.; Rauk, A.; Tschuikow-Roux, E. *J. Phys. Chem.* **1991**, *95*, 9900.
(22) Jodkowski, J.; Rayez, M.-T.; Rayez, J.-C.; Bérces, T.; Dóbé, S. *J. Phys. Chem. A* **1998**, *102*, 9219.
(23) Greenwald, E. E.; North, S. W.; Georgievskii, Y.; Klippenstein, S. J. *J. Phys. Chem. A* **2005**, *109*, 6031.
(24) Matsumoto, K.; Klippenstein, S. J.; Tonokura, K.; Koshi, M. *J. Phys. Chem. A* **2005**, *109*, 4911.
(25) Lee, C.; Luther, K.; Oum, K.; Troe, J. *J. Phys. Chem. A* **2006**, *110*, 2613.
(26) Luther, K.; Oum, K.; Sekiguchi, K.; Troe, J. *Phys. Chem. Chem. Phys.* **2004**, *6*, 4133.
(27) Oum, K.; Luther, K.; Troe, J. *J. Phys. Chem. A* **2004**, *108*, 2690.
(28) Xu, S. C.; Zhu, R. S.; Lin, M. C. *Int. J. Chem. Kinet.* **2006**, *38*, 322.
(29) Krasnoperov, L. V.; Peng, J.; Marshall, P. *J. Phys. Chem. A* **2006**, *110*, 3110.
(30) Miller, W. H.; Handy, N. C.; Adams, J. E. *J. Chem. Phys.* **1980**, *72*, 99.
(31) Rai, S. N.; Truhlar, D. G. *J. Chem. Phys.* **1983**, *79*, 6046.
(32) Hase, W. L.; Mondro, S. L.; Duchovic, R. J.; Hirst, D. M. *J. Am. Chem. Soc.* **1987**, *109*, 2916.
(33) Guadagnini, R.; Schatz, G. C.; Walch, S. P. *J. Phys. Chem. A* **1998**, *102*, 5857.
(34) Klippenstein, S. J. *J. Chem. Phys.* **1992**, *96*, 367.
(35) Klippenstein, S. J. *J. Chem. Phys.* **1994**, *101*, 1996.
(36) Georgievskii, Y.; Klippenstein, S. J. *J. Phys. Chem. A* **2003**, *107*, 9776.
(37) Georgievskii, Y.; Klippenstein, S. J. *J. Chem. Phys.* **2003**, *118*, 5442.
(38) Harding, L. B.; Georgievskii, Y.; Klippenstein, S. J. *J. Phys. Chem. A* **2005**, *109*, 4646.
(39) Klippenstein, S. J.; Georgievskii, Y.; Harding, L. B. *Phys. Chem. Chem. Phys.* **2006**, *8*, 1133.
(40) Georgievskii, Y.; Klippenstein, S. J. *J. Chem. Phys.* **2005**, *122*, 194103.
(41) Hess, W. P.; Durant, J. L., Jr.; Tully, F. P. *J. Phys. Chem.* **1989**, *93*, 6402.
(42) Atakan, B.; Wolfrum, J. *Chem. Phys. Lett.* **1991**, *186*, 547.
(43) Balla, R. J.; Castleton, K. H. *J. Phys. Chem.* **1991**, *95*, 2344.
(44) Bullock, G. E.; Cooper, R. E. *J. Chem. Soc., Faraday Trans. I* **1972**, *68*, 2185.
(45) Rowe, B. R.; Dupeyrat, G.; Marquette, J. B.; Gaucherel, P. *J. Chem. Phys.* **1984**, *80*, 4915.
(46) Drzaic, P. S.; Marks, J.; Braumann, J. I. In *Gas-phase ion chemistry*; Bowers, M. T., Ed.; Academic Press: New York, 1984; Vol. 3, Chapter 21.
(47) Smith, I. W. M. *Int. J. Mass Spectrom. Ion Processes* **1995**, *149*, 231.
(48) Hampel, C.; Peterson, K.; Werner, H.-J. *Chem. Phys. Lett.* **1992**, *190*, 1.

(49) Knowles, P. J.; Hampel, C.; Werner, H.-J. *J. Chem. Phys.* **2000**, *112*, 3106.
(50) Werner, H.-J. *Mol. Phys.* **1996**, *89*, 645.
(51) Celani, P.; Werner, H.-J. *J. Chem. Phys.* **2000**, *112*, 5546.
(52) Werner, H.-J.; Knowles, P. J.; Lindh, R.; Schütz, M.; P. Celani, T. K.; Manby, F. R.; Rauhut, G.; Amos, R. D.; Bernhardsson, A.; Berning, A.; Cooper, D. L.; Deegan, M. J. O.; Dobbyn, A. J.; Eckert, F.; Hampel, C.; Hetzer, G.; Lloyd, A. W.; McNicholas, S. J.; Meyer, W.; Mura, M. E.; Nicklass, A.; Palmieri, P.; Pitzer, R.; Schumann, U.; Stoll, H.; Stone, A. J.; Tarroni, R.; Thorsteinsson, T. Molpro, version 2002.10, a package of ab initio programs.
(53) Celani, P.; Werner, H.-J. *J. Chem. Phys.* **2003**, *119*, 5044.
(54) Dunning, T. H., Jr. *J. Chem. Phys.* **1989**, *90*, 1007.
(55) For example, this geometry affects the RCCSD(T) saddle point barrier height by less than 0.004 kcal/mol.
(56) Lee, T. J.; Rendell, A. P.; Taylor, P. R. *J. Phys. Chem.* **1990**, *94*, 5463.
(57) Werner, H.-J.; Knowles, P. J. *J. Chem. Phys.* **1985**, *82*, 5053.
(58) Knowles, P. J.; Werner, H.-J. *Chem. Phys. Lett.* **1985**, *115*, 259.
(59) Knowles, P. J.; Hampel, C.; Werner, H.-J. *J. Chem. Phys.* **1993**, *99*, 5219.
(60) Feller, D.; Dixon, D. A. *J. Chem. Phys.* **2001**, *115*, 3484.
(61) Martin, J. M. L. *Chem. Phys. Lett.* **1996**, *259*, 669.
(62) Sun, J.; Ruedenberg, K. *J. Chem. Phys.* **1993**, *99*, 5269.
(63) Eckert, F.; Werner, H.-J. *Theor. Chem. Acc.* **1998**, *100*, 21.
(64) Villà, J.; Truhlar, D. G. *Theor. Chem. Acc.* **1997**, *97*, 317.
(65) Corchado, J. C.; Chuang, Y.-Y.; Fast, P. L.; Hu, W.-P.; Liu, Y.-P.; Lynch, G. C.; Jackels, K. A. C. F.; Ramos, A. F.; Ellingson, B. A.; Lynch, B. J.; Melissas, V. S.; Vill, J.; Rossi, I.; Coitio, E. L.; Pu, J.; Albu, T. V.; Steckler, R.; Garrett, B. C.; Isaacson, A. D.; Truhlar, D. G. Polyrate - version 9.4.; University of Minnesota: Minneapolis, 2005.
(66) Conserved modes are those that do not change their identity in the course of the reaction. They include free fragments vibrations.
(67) Frisch, M. J.; Trucks, G. W.; Schlegel, H. B.; Scuseria, G. E.; Robb, M. A.; Cheeseman, J. R.; Zakrzewski, V. G.; Montgomery, J. A.; Stratmann, R. E.; Burant, J. C.; Dapprich, S.; Millam, J. M.; Daniels, A. D.; Kudin, K. N.; Strain, M. C.; Farkas, O.; Tomasi, J.; Barone, V.; Cossi, M.; Cammi, R.; Mennucci, B.; Pomelli, C.; Adamo, C.; Clifford, S.; Ochterski, J.; Petersson, G. A.; Ayala, P. Y.; Cui, Q.; Morokuma, K.; Malick, D. K.; Rabuck, A. D.; Raghavachari, K.; Foresman, J. B.; Cioslowski, J.; Ortiz, J. V.; Stefanov, B. B.; Liu, G.; Liashenko, A.; Piskorz, P.; Komaromi, I.; Gomperts, R.; Martin, R. L.; Fox, D. J.; Keith, T.; Al-Laham, M. A.; Peng, C. Y.; Nanyakkara, A.; Gonzalez, C.; Challacombe, M.; Gill, P. M. W.; Johnson, B.; Chen, W.; Wong, M. W.; Andres, J. L.; Gonzalez, C.; Head-Gordon, M.; Replogle, E. S.; Pople, J. A. *Gaussian 98*; Gaussian Inc.: Pittsburgh, PA, 1998.
(68) Møller, C.; Plesset, M. C. *Phys. Rep.* **1934**, *46*, 618.
(69) Amos, R. D.; Andrews, J. S.; Handy, N. C.; Knowles, P. J. *Chem. Phys. Lett.* **1991**, *185*, 256.
(70) Singleton, D. L.; Cvetanovic, R. J. *J. Am. Chem. Soc.* **1976**, *98*, 6812.
(71) Alvarez-Idaboy, J. R.; Mora-Diez, N.; Vivier-Bunge, A. *J. Am. Chem. Soc.* **2000**, *122*, 3715.
(72) Quack, M.; Troe, J. *Ber. Bunsen-Ges. Phys. Chem.* **1975**, *79*, 170.